P7.1 STUDY ON THE OPTIMAL SCANNING STRATEGIES OF PHASE-ARRAY RADAR THROUGH ENSEMBLE KALMAN FILTER ASSIMILATION OF SIMULATED DATA

Ting Lei[1], Ming Xue[1,2] , Tianyou Yu[3] and Michihiro Teshiba[3]
[1]Center for Analysis and Prediction of Storms
[2]School of Meteorology
and [3]School of Electrical and Computer Engineering
University of Oklahoma

1. Introduction

The phased-array radar (PAR) of the National Weather Radar Testbed (NWRT) in Norman, Oklahoma represents a paradigm shift for weather radar observations. The PAR with abilities such as a higher data update rate through beam multiplexing (Yu et al. 2007) offers not only an opportunity but also a challenge for meteorologists to exploit its potentials for helping us improve convective storm analysis and prediction. In this paper, the ensemble Kalman filter (EnKF) data assimilation technique is used to study the impact of different scanning strategies and to provide scientific guidance for the design and use of optimal scanning strategies for PAR.

The EnKF method has shown great promise in a number of recent studies with simulated data within the Observation Simulation System Experiments, (OSSE, Snyder and Zhang 2003; Zhang et al. 2004; Tong and Xue 2005, TX05 hereafter; Xue et al. 2006, XTD06 hereafter). These OSSE studies, especially the earlier ones, make several simplifying assumptions about radar observations. For example, radar data are assumed to be available on the regular model grid points in the first three studies referenced. XTD06 assumes that radar data are available in the PPI planes but at vertical columns that coincides with columns of the analysis grid. In this study, the ARPS (Advanced Regional Prediction System) EnKF data assimilation system is upgraded to directly assimilate flexible forms of radar data, such as those on individual radials, and to apply more realistic observation operators that include beam weighting in all three directions. A companion radar emulator has been developed to simulate various scanning modes of PAR and produce realistically simulated data. As a result, in this system, OSSE for different scanning strategies can be easily implemented.

In the experiments reported here, in both the truth simulation and data analysis, the same grid is used with a horizontal grid spacing of 1 km and a stretched vertical grid of 100 m at the surface while increasing to 900 m at the model top. A perfect assimilating model is assumed.

This paper is organized as follows: in second 2, the EnKF systems and simulated radar data are briefly described. In section 3, OSS experimental design and some important parameter options in the ARPS EnKF system are described and the experiment results are presented. Discussions are given in section 4.

2. EnKF system and simulated radar observations

The ARPS EnKF system used in this paper is an upgraded version of that described by TX05 and XTD06. The main new feature is its added ability to handle radar observations in radar coordinates, which is necessary to study the impact of various scanning strategies, including azimuthal and vertical oversampling. A more realistic 3D volume average approach is also added as an option in the radar observation operator.

The formulas that relate radial velocity and reflectivity to atmospheric state variables are the same as described in TX05. We describe here only the volume average aspect that is different from TX05 and XTD06. For reflectivity at the center of radar sampling volume,

$$\eta(r_0,\theta_0,\phi_0)=\frac{\sum_{vol}\eta_{i,j,k}\left|W\left(r_{i,j,k}\right)\right|^2 f^4\left(\theta_{i,j,k},\phi_{i,j,k}\right)}{\sum_{vol}\left|W\left(r_{i,j,k}\right)\right|^2 f^4\left(\theta_{i,j,k},\phi_{i,j,k}\right)}, \qquad (1)$$

and for the corresponding radial velocity,

$$v(r_0,\theta_0,\phi_0)=\frac{\sum_{vol}v_{i,j,k}\left|W\left(r_{i,j,k}\right)\right|^2 f^4\left(\theta_{i,j,k},\phi_{i,j,k}\right)}{\sum_{vol}\left|W\left(r_{i,j,k}\right)\right|^2 f^4\left(\theta_{i,j,k},\phi_{i,j,k}\right)}, \qquad (2)$$

where $v_{i,j,k}$ and $\eta_{i,j,k}$ were the radial velocity and reflectivity at grid point (i, j, k) located within the radar volume centered at (r_0,θ_0,ϕ_0). Compared to standard formulas, such as Eq. (5.48) of Doviak and Zrnic' (1993, DZ93 hereafter),, the reflectivity weighting in (2) is neglected.

Corresponding author address: Ting Lei, Center for Analysis and Prediction of Storms,120 David L. Boren Blvd., Norman, OK 73072.
E-mail: tlei@ou.edu

The resolution of the truth simulation is 1 km in the horizontal. To avoid having many gates that contain no grid point, we assume that radar gate spacing is 1 km instead of the actual 250 m of the PAR. The range weighting function, $W(r)$, has the following form:

$$W(r_{i,j,k}) = \begin{cases} 1, & |r_{i,j,k} - r_0| \le 1.5r_6 \\ W_t\left(|r_{i,j,k} - r_6| - 1.5r_6\right), & |r_{i,j,k} - r_0| > 1.5r_6 \end{cases}, \quad (3)$$

where W_t has the same functional form as given by Eq. (11.118) of DZ93:

$$|W_t(dr)|^2 = \exp\left[-(dr)^2 / 2\sigma_r^2\right], \quad (4)$$

where, from Eq. (5.76) of DZ93,

$$\sigma_r^2 = (0.30r_6)^2, \quad (5)$$

and r_6 is taken as 235 m as in Wood and Brown (1997), a parameter based on the WSR-88D radars.

For azimuth and elevation weighting Eq. (A.3) of Wood and Brown (1997):

$$f^4(\theta_{i,j,k}, \phi_{i,j,k}) = \exp\left\{-4\ln 4\left[\left(\frac{\theta_{i,j,k} - \theta}{\theta_w}\right)^2 + \left(\frac{\phi_{i,j,k} - \phi}{\phi_w}\right)^2\right]\right\}, \quad (6)$$

θ_w and ϕ_w are beam width in azimuth and elevation respectively, and their values will be specified for individual experiments.

As in XTD06, the beam bending and earth curvature effort is taken into account therefore height of the lowest-elevation beam above ground increases with radar range, resulting in an increased loss of low-level coverage as the storm is further away from the radar.

3. OSSE design, EnKF configuration and results

a. OSSE design

In present work, the model errors are not considered. In both the truth simulation and analysis system, the horizontal resolutions are 1 km, and the vertical grid spacing increases from 100 m at the surface to 900 m at the model top. The model domain 64 × 64 × 20 km and there 43 levels in the vertical.

The truth simulation uses the May 20, 1977 Del City Oklahoma sounding (Xue et al 2001). The Smagrinsky turbulence closure scheme is used, together with Lin ice microphysics. The model storm is triggered by a thermal bubble placed at the low level of a horizontally homogeneous environment, and the model is integrated for two hours. The simulated storm evolution is similar to that in Xue et al. (2001). Similar truth simulations were used in TX05 and XTD06.

As mentioned in the introduction, this work focuses on the impact of scanning strategies when the radar observations are potentially insufficient in spatial resolutions, which can occur when the radar is located as a large distance from the storms. In this study, we examine radar locations at (- 100, 0), (- 80, 0), (- 60, 0) and (- 40, 0)km where (0, 0)km is at the lower left corner of the model grid. The main storm cell, or the right moving cell after storm splitting, is located close to the domain center at (32, 32) km.

In addition, two benchmark experiments with radar positions at (-100, 0)km and (0, 0)km, respectively, are conducted, in which the radar observations are assumed to be taken at the scalar points of the model grid. These experiments serve as the benchmarks and represent the optimal scenario where no horizontal interpolation or radar volume averaging is involved. This is also the assumption made in TX05 and in Snyder and Zhang (2003) and Zhang et al. (2004).

In our experiment, the gate spacing is 1 km. Two radar beam widths of 2^o or 1^o are considered, with angular (in azimuth and/or in elevation) sampling increments of 2^o, 1^o or 0.5^o. When the sampling increment is smaller than the beam width, we call it over-sampling in the corresponding direction. In other words, angular over-sampling occurs if then beam width is larger than its' increments. Specific configurations of these parameters are listed for different experiments in Table1.

b. ARPS EnKF configuration

In this work, the ensemble square root filter (EnSRF) scheme is used, as in XTD06. Both radial velocity and reflectivity are assimilated starting from the first analysis cycle. The reflectivity is assimilated starting from the first cycle, following Tong and Xue (2007).

As in TX05 and XTD06, the initial ensemble forecast starts at 20 min of model time, and the first analysis occurs at 25 min. The initial ensembles are specified by adding smoothed random perturbations to the initial guess defined by the truth simulation sounding. A discussion on the smoothed perturbation can be found in Tong and Xue (2007). Again following XTD06, fourty ensemble members are used. More members usually do not significantly improve the results but increases the computational cost.

For all experiments, the covariance inflation coefficient is taken as 1.1, which is found to work the best. Covariance location is applied in the same way as in TX05 and XTD06, using a Schur product to the calculated covariance. A localization cut-off radius of 4 km in all directions for reflectivity analysis is found

to work generally the best and is therefore used in all experiments reported here.

Table 1. List of experiments.

Categories / Parameters	W2I2	W2I1	W2I0.5	N88d	W2I2-HF	W2I1-HF
Beam width	2°	2°	2°	1°	2°	2°
Angular increment in athimuth/elevation	2°	1°	0.5°	1°	2°	1°
Lowest elevation	1°	1°	1°	0.5°	1°	1°
Volume scan interval	5 min	5 min	5 min	5 min	1.25 min	1.25 min

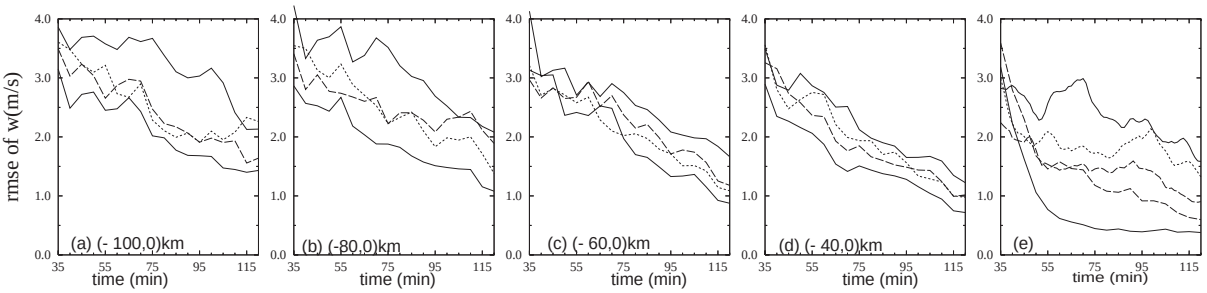

Fig. 1. The rms errors of ensemble mean analyses of vertical velocity w, averaged over points at which the true reflectivity is greater than 5 dBZ for radar locations (-100, 0) (a), (-80, 0) (b), (-60, 0)(c) and (-40, 0)km (d) respectively. In (a-d), the lower solid line is for experiment N88d, dashed for W2I1, dotted for W2I0.5 and upper solid for W2I2. In (e), high frequency update experiments (dotted line for W2I1-HF with radar coordinates (-100, 0) km, upper dashed line for W2I1-HF with radar coordinates (-60, 0)km, and benchmark experiments (lower solid line for radar coordinates (0,0)km and lower dashed line for radar coordinate (-100,0)km experiments.

c. Results

As shown in Table 1, there are 6 categories of experiments for the case of radar data on radials. For each category, there are 4 experiments with different radar positions of (-100, 0), (-80, 0), (-60, 0) and (0, 0)km. We name the experiments using the x-coordinate of the radar location and the category names in Table 1. For example, 60-W2I1 represents experiment W2I1 with radar located at (- 60, 0) km.

For all simulated radar observations, random errors drawn from Gaussian distributions of zero mean and standard deviations of 1 m s^{-1} and 2 dBZ for radial velocity and reflectivity, respectively, are added to the observations.

The rms errors of the analyzed vertical velocity through the analysis cycles are shown in Fig. 1 for several experiments. The benchmark experiments with radar positions at (-100, 0) and (0, 0) km in Fig. 1e exhibit, not surprisingly, the best performance, compared to experiments whose data are sampled on the radials, because of absence of horizontal interpolation or volume average error. The differences between the two benchmark experiments must have been due to the difference in the amount of vertical velocity components observed. For this reason, the analyzed w errors in the cases with radar at (0, 0) are smaller.

In all these experiments, except for 100-W2I2 and 80-W2I2, the analyses are brought closer to the truth continuously through the 5-min assimilation cycles. The lowest level of error is generally found at the end of the data assimilation window. As an example, a qualitative comparison of 100-W2I1 and the truth is shown in Fig. 2,3. It is seen that the storm evolution is basically captured by 100-W2I1. For these cases, the ability of EnKF in recovering the model states through a large number of data assimilation cycles is demonstrated for the situations of insufficient resolution and the lack of low-level observations, due to the elevation and earth curvature effects. But clearly, such effects slow down the error reduction.

As shown in Fig. 1, experiment W2I2 with a two degree beam width and two degree increments shows the worst results for a given radar position. Among the experiments with data on radials, N88d, which has a 1 degree beam width and 1 degree increment, shows the best performance. Experiments W2I1 and W2I0.5, which over-sample by a factor of 2 and 4, respectively, exhibit clearly improved results compared to W2I2, which does not perform oversampling. This demonstrates the potential of using the over-sampling strategy for improving observation resolution and storm-analysis accuracy. It should be noted that this performance is obtained when W2I1 and W2I0.5 start their first elevation at 1 degree, while N88d starts at 0.5°. Therefore N88d not only has the benefit of narrow beams, but also the benefit of being able to cover lower levels directly. The 1°

first level is dictated by the 2° beam width. An elevation lower than half of the beam width should be avoided to avoid excessive ground cluster.

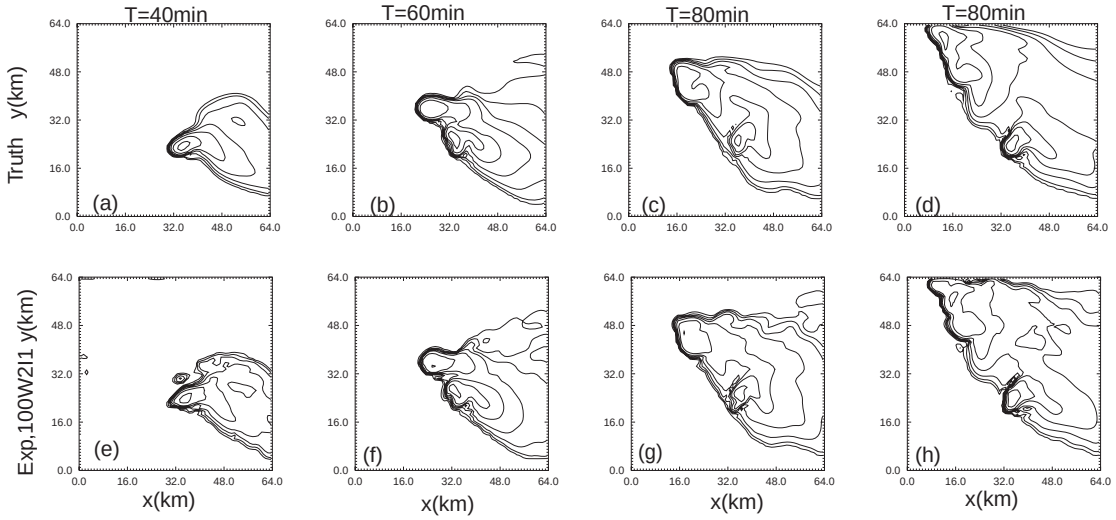

Fig. 2. Horizontal cross sections of reflectivity at 6 km above ground, for the truth (a-d), and and experiment 100M2I1 (e-h), at 40, 60, 80 and 100 min. Contour interval is 10 dBZ.

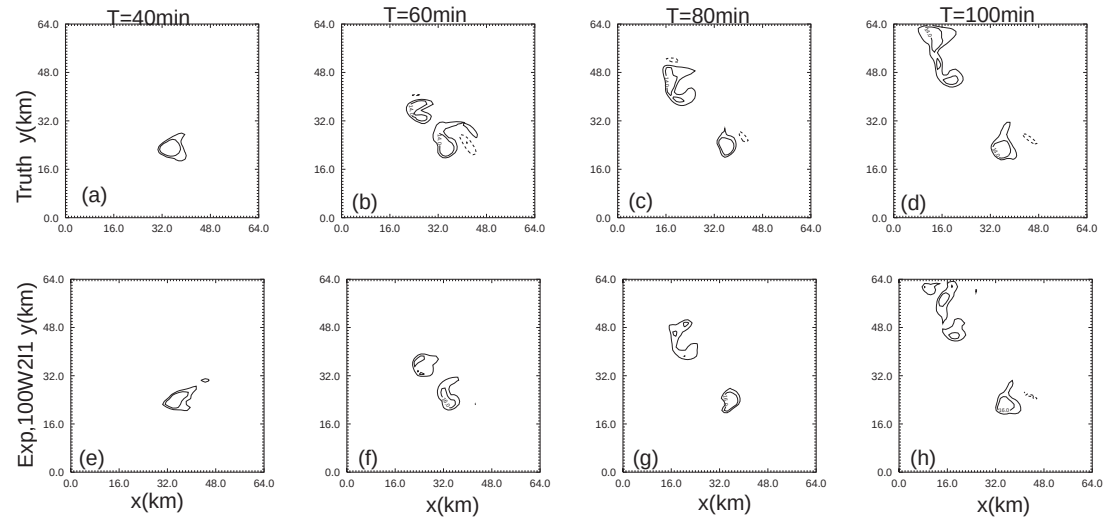

Fig. 3. As Fig. 2 but for vertical velocity. Contour interval is 7 ms^{-1}.

However, W2I0.5, which uses over-sampling with a 0.5° angular increment in both azimuth and elevation directions and therefore 4 times as many observations, does not show clear and consistent improvements over the results of W2I1,,though,rms errors of the former are normally smaller than those of the latter at least at the end of data assimilation. An exception is results of experiments with radar located at (-100, 0)km (Fig.1a), in which the ms errors of vertical velocity are larger than those of W2I1. Fig. 1a shows that at the end of data analysis, the results of 100-W2I0.5 are worse than those of 100W2I1. These results indicate that for a given beam width and a given analysis grid resolution, there is a lower limit to the sampling increment, beyond which little additional gain is obtained. This is especially the case, when weather of interest is located far from the radar and the cross-beam resolution becomes coarse.

From Fig. 1, by comparing experiments with 5-min volume scan interval to the benchmark experiments, it is clear that, in addition to having larger rms errors at the end of data assimilation window, the rms errors decrease much slower during the early and intermediate assimilation cycles. These results show the benefit of faster volume scan, in accelerating the error reduction through assimilation cycles. For

newly developed thunderstorms that have not had radar data available for long, the faster volume scans means more accurate analysis in a shorter period of time, and more accurate predictions. Being able to perform faster volume scans, via, e.g., beam multiplexing (Yu et al. 2007), is a clear advantage of phased-array radars. Additional benefit is achieved by combining faster scans and spatial over-sampling.

The differences between the vertical velocity rms errors of 40W2I1 and 60W2I1, and of 80W2I1 and 100W2I1, are very small. Thus, only one from a certain pair of results are plotted in Fig.1e. It should be noted that 100W2I2-HF, without over-sampling, shows almost no improvement over W2I2.

4. Discussion

This work combines the promising EnKF data assimilation method with a more realistic representation of radar sampling volume averaging in the radar observation operators in both the EnKF system and its companion emulator, to study the effects of different potential scanning strategies of PAR. In the preliminary work reported here, the advantages of oversampling and fast volume scans possible with the PAR are demonstrated.

The present work is conducted under the condition of perfect model, in which the truth simulation and data analysis use identical prediction model. The results obtained using perfect models tend to be overoptimistic. The inclusion of model resolution and physics errors will be considered in our future studies, so will the use of higher analysis grid resolutions, which is likely to benefit more from the spatial oversampling.

Acknowledgement This work is primarily supported by ONR EPSCOR Program grant DOD-ONR N00014-06-1-0590. The first author would like to thank Drs. Mingjing Tong and Keith Brewster for their helps with code development.

References

Snyder, C., and F. Zhang, 2003: Assimilation of simulated Doppler radar observations with an ensemble Kalman filter. *Mon. Wea. Rev.*, **131,** 1663-1677.

Tong, M., and M. Xue, 2005: Ensemble Kalman filter assimilation of Doppler radar data with a compressible nonhydrostatic model: OSS Experiments. M*on. Wea. Rev.*, **133,**1789-1807.

Tong, M. and M. Xue, 2007: Simultaneous estimation of microphysical parameters and atmospheric state with radar data and ensemble square-root Kalman filter. Part I: Sensitivity analysis and parameter identifiability *Mon. Wea. Rev.***,** Conditionally accepted.

Xue, M., K. K. Droegemeier, V. Wong, A. Shapiro, K. Brewster, F. Carr, D. Weber,Y. Liu, and D.-H. Wang, 2001: The Advanced Regional Prediction System (ARPS) - A multiscale nonhydrostatic atmospheric simulation and prediction tool. Part II: Model physics and applications. M*eteor. Atmos. Phy.*, 7**6,** 143-165.

Xue, M., M. Tong, and K. K. Droegemeier, 2006: An OSSE framework based on the ensemble sqaure-root Kalman filter for evaluating impact of data from radr networks on thunderstorm analysis and forecast. J.Atmos. Oceanic Technol., **23**,46-66.

Yu, T., M. B. Orescanin, C. D. Curtis, D. S. Zrnic, and D. E. Forsyth, 2007: Beam multiplexing using the phased-array weather radar. *J. Atmos. Oceanic Technol.*, **24**, 103–118.

Zhang, F., C. Snyder, and J. Sun, 2004: Impacts of initial estimate and observations on the convective-scale data assimilation with an ensemble Kalman filter. M*on. Wea. Rev.*, 1**32,** 1238-1253.